30th NENE 2021
September 6 - 9
BLED-SLOVENIA
International Conference Nuclear Energy for New Europe

Simulation of heat transfer in multiple impinging jets with scale-adaptive turbulence model

Martin Draksler, Matej Tekavčič, Boštjan Končar
Jožef Stefan Institute
Jamova cesta 39
SI-1000 Ljubljana, Slovenia
martin.draksler@ijs.si, matej.tekavcic@ijs.si, bostjan.koncar@ijs.si

ABSTRACT

The capability of standard k- ω SST and scale-adaptive SST-SAS turbulence models to predict the turbulence and heat transfer of multiple impinging jets is analysed. The investigated case considers 13 symmetrically arranged turbulent impinging jets at inlet Reynolds number of around 20000 and nozzle-to-plate distance equal to four. The numerical simulations have been performed with the open-source code OpenFOAM and validated against the well-resolved LES results. The results have shown that the SST-SAS model exhibits the same high level of dissipation as the standard SST model. In comparison to the LES benchmark, both, SST and SAS-SST models predict higher eddy viscosity values and higher heat transfer rates.

1 INTRODUCTION

Though the main features of the jet impingement flow can be reproduced by the time-averaged models, the transient phenomena play a decisive role in the heat transfer prediction on the impingement (heated) surface. These have been rather accurately simulated in our previous studies using the Large Eddy Simulation (LES) [1]. But LES approach requires large amount of computational resources that are hardly affordable, especially in the case of multiple jets. The need for less expensive, but still transient turbulence models is therefore obvious.

A relatively good prediction for the first and second order flow statistics and turbulence budgets can be obtained by computationally less demanding unsteady Reynolds averaged Navier-Stokes (URANS) approach [2]. However, URANS simulations in combination with the conventional eddy-viscosity turbulence models (e.g. Shear Stress Transport (SST) model) tend to suppress the flow instabilities in the shear layer of individual jets that govern the unsteady jet dynamics near the heated surface. Flow unsteadiness might be better captured with the SST-based Scale-Adaptive Simulation model (SST-SAS model) [3], which has the capability to detect the local flow unsteadiness and adapt the turbulence quantities (turbulence kinetic energy k and eddy viscosity ω) in these regions. This results in local reduction of eddy viscosity and allows the flow instability to develop.

The objective of this study is to analyze and evaluate the predictive capability of SST and SST-SAS models with respect to turbulence and heat transfer. A sensitivity study regarding the specified turbulent Prandtl number was performed to demonstrate the change in heat transfer prediction with respect to changes in effective thermal diffusivity. Investigated case considers the configuration with 13 turbulent impinging jets at inlet Reynolds number of around 20000 [4]. The numerical simulations are conducted with the open-source CFD code OpenFOAM and validated against the well-resolved LES results [5].

2 SIMULATED CASE

The flow of impinging jets is considered to be three-dimensional and incompressible. Governing equations for the fluid motion, consisting of continuity and momentum equations, and heat transfer equation are numerically solved by the Finite Volume (FV) method on collocated grid, using an open-source CFD code OpenFOAM v1812 [6]. The flow is resolved using the unsteady Reynolds-averaged Navier-Stokes (URANS) approach. Two different turbulence modelling approaches were adopted, namely the Shear Stress Transport (SST) model [7] and the Scale Adaptive Simulation (SST-SAS) [8] model. The essential difference between SST-SAS and SST models stems from an additional SAS source term P_{SAS} in the turbulence specific dissipation rate ω equation:

$$P_{SAS} = max\left[\left(\rho\zeta_2 S^2\left(\frac{L}{L_{vK}}\right)^2 - C_{SAS}\frac{2\rho k}{\sigma_\Phi} max\left(\frac{1}{k^2}\frac{\partial^2 k}{\partial \mathrm{x}_j^2}, \frac{1}{\omega^2}\frac{\partial^2 \omega}{\partial \mathrm{x}_j^2}\right), 0\right)\right], \quad (1)$$

where ρ is the density and k is the turbulence kinetic energy. The model parameters in the SAS source term are $\zeta_2 = 3.51$, $\sigma_\Phi = 2/3$ and $C_{SAS} = 2$. The variable L represents the modelled turbulent length scale $L = k^{1/4}/\left(C_\mu^{1/4}\omega\right)$. The L_{vK} denotes the von Kármán length scale, which is proportional to the von Kármán constant $\kappa = 0.41$ and the ratio of the first and the second velocity derivatives:

$$L_{vK} = \frac{\kappa S}{|\partial^2 \bar{U}_i / \partial \mathrm{x}_j^2|} \quad (2)$$

The first velocity derivative is represented by the magnitude $S = \sqrt{2S_{ij}S_{ij}}$, where S_{ij} is the strain rate tensor $S_{ij} = 1/2\ (\partial\bar{U}_i/\partial x_j + \partial\bar{U}_j/\partial x_i\ )$ and $\bar{U}_i$ is the Reynolds averaged velocity in *i*-th direction. A detailed description of the SST-SAS model is given in [9].

The heat equation solved to resolve the cooling by turbulent impinging jets can be written as shown in Eq. (3) below:

$$\frac{\partial T}{\partial t} + \nabla(\bar{\boldsymbol{U}}T) + \nabla(\alpha_{\mathrm{eff}}\nabla T) = 0, \quad (3)$$

where T is the temperature. The effective heat diffusivity

$$\alpha_{\mathrm{eff}} = \alpha + \alpha_{\mathrm{t}} = \frac{\nu}{\mathrm{Pr}} + \frac{\nu_{\mathrm{t}}}{\mathrm{Pr}_{\mathrm{t}}} \quad (4)$$

combines the molecular heat diffusivity α and turbulent heat diffusivity α_{t}. Air properties at 20°C are used to set the molecular kinematic viscosity ν and Prandtl number Pr. Turbulent eddy viscosity is given by the turbulence model used, while the turbulent Prandtl number Pr_t is set to 0.9. The effects of turbulence modelling on heat transfer prediction are examined in section 3.

2.1 Domain, mesh and flow conditions

The computational domain is presented in Figure 1. The fluid enters the domain through the nozzle plate (inlet) and leaves the domain through four vertical boundary planes (outlet). The nozzle diameter D is equal to 0.013 m, with the pitch-to-pitch distance s/D equal to two, and the nozzle-to-plate distance equal to four nozzle diameters. Detailed description of the simulation case (including LES setup) can be found in [1], [4] and [5]. Origin of the coordinate

system is located at the geometric center of the target plate, with the y-axis pointing towards the nozzle plate. The U and W denote the wall-parallel velocity components (in x and z directions), while V denotes the axial velocity (in y direction). Numerical results are presented in characteristic plane P-1 which intersects the axes of the central jet and one of its closest neighbour jet.

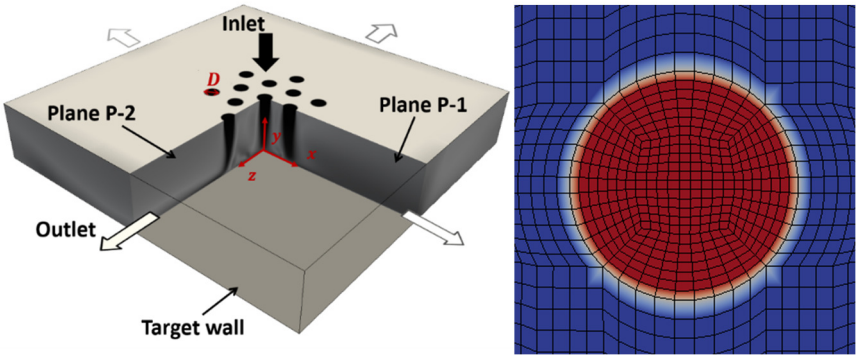

Figure 1: Computational domain (left). Close-up view of the grid topology in the jet (right).

Flat velocity profile with the turbulence intensity of 10% is prescribed at the domain inlet while zero gradient boundary condition is used at the outlet. Both, the nozzle plate and the target surface are modelled as no-slip walls. The Neumann boundary condition for pressure is used at all boundaries where the velocity is prescribed, and the pressure at the outlet is set to zero.

The transient solution is obtained using the PISO algorithm [10]. The temporal discretization is obtained with the second order accurate Backward scheme. Spatial discretization is obtained with second order schemes for velocity, and first order schemes for temperature and turbulence. The PISO algorithm used adaptive time step, based on the Courant-Friedrichs-Lewy (CFL) number kept equal/below unity to achieve the solver convergence.

2.2 Mesh sensitivity study

Mesh sensitivity study included three different numerical meshes, with total number of cells ranging from 1550217 to 3238684. Fully structured hexa grids were built in ANSYS ICEM CFD meshing tool [11], with the so-called "O-grid" meshing applied to all blocks corresponding to jet locations (see Figure 1 right). Grid spacing in both wall-parallel (x and z) directions is kept relatively uniform in the central region of the computational domain, while grid refinement in vertical direction towards both plates is applied, aiming to achieve a desired grid resolution especially near the target plate. The grid topology is kept similar for all tested grids - only the number of grid nodes in particular direction and/or the size of the first near-wall cells next to the target plate is varied. The information on tested numerical grids is summarized in Table 1.

Table 1: Grid summary

	# cells (total)	# cells across jet	# cells between jets	# cells (vertical)	First node distance from target wall [m]	Y^+_{max} (dimension-less wall distance)
Grid 1	1550217	23	17	80	2.5×10^{-5}	4.7
Grid 2	3238684	30	30	80	5.0×10^{-6}	1.0
Grid 3	3238684	30	30	80	2.5×10^{-6}	0.5

3 RESULTS AND DISCUSSION

The presented URANS simulation results are compared to the time-averaged results from well-resolved LES benchmark case [5]. Transient URANS results are averaged over the one second of physical time, and additionally across six rotational symmetries. All URANS simulations were run with the turbulent inlet intensity set to 10%, and without using any wall functions. In our previous study [3], it has been shown that "sufficiently far above the target plate" both the SST-SAS and SST models predict a very similar formation of individual jet. Thus, in this study the flow characteristics are analysed in a close vicinity of the target wall, i.e. at $y/D = 0.0125$. Results of the mesh sensitivity study are shown in Figure 2, where radial profiles of mean axial velocity V/V_{cl}, normalized eddy viscosity ν_t/ν and mean turbulence kinetic energy k/V_{cl}^2 at $y/D = 0.0125$ above the target plate in plane P-1 are presented. In parallel, the averaged wall temperature (i.e. the impingement plate temperature) is shown.

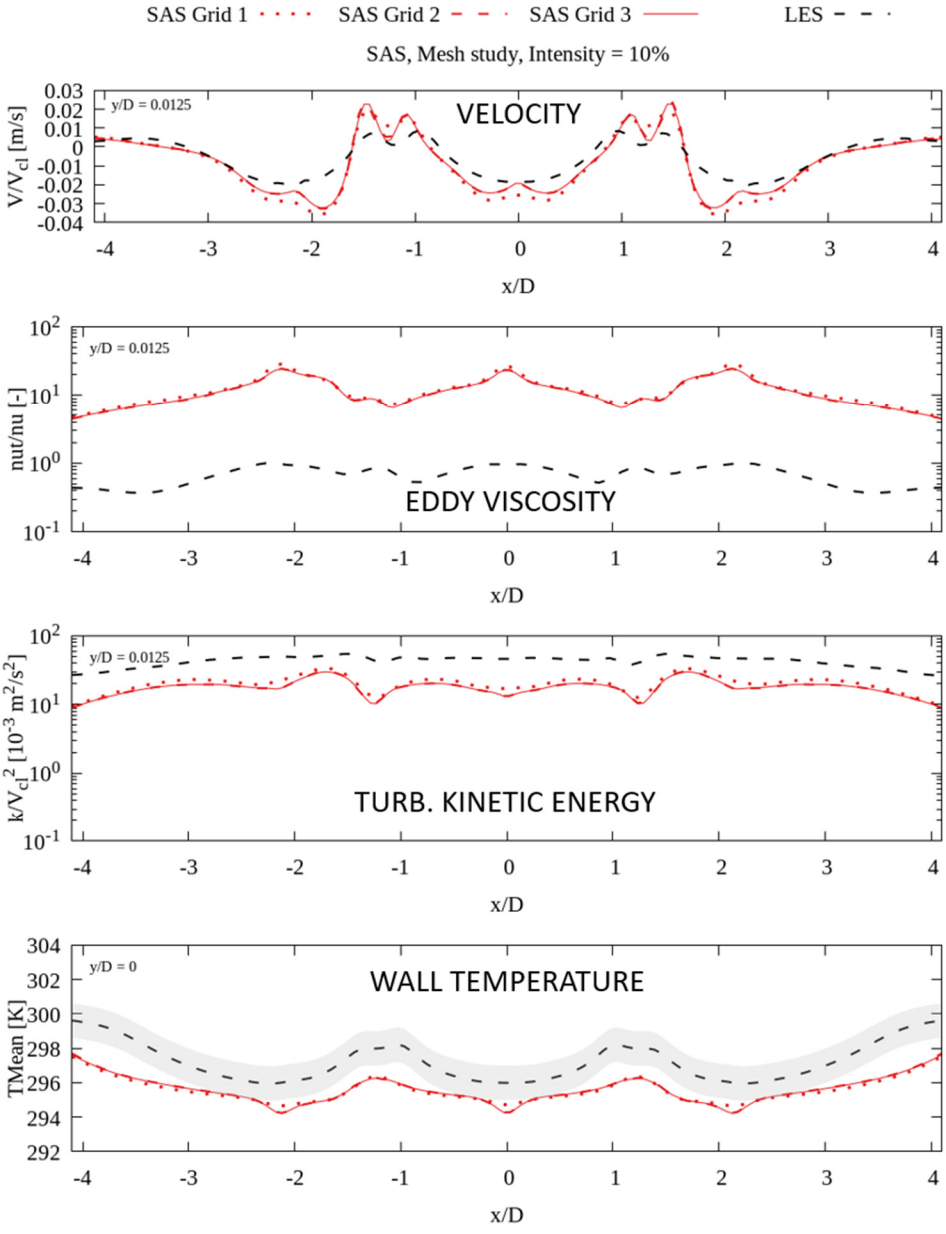

Figure 2: Mesh sensitivity study with SAS model. Profiles of mean axial velocity V/V_{cl}, normalized mean eddy viscosity ν_t/ν and mean turbulence kinetic energy k/V_{cl}^2 are extracted at $y/D = 0.0125$ above the target plate. Profiles of mean wall temperature are shown as well.

The main difference between the tested meshes is observed in the stagnation region of individual jet (i.e. at locations where the jets impinge the wall), where somewhat "higher jet" velocity is obtained with the coarsest mesh Grid 1. It may be also observed that the secondary stagnation zones where adjacent jets collide are not sufficiently resolved with the Grid 1 which has approximately 2 times lower node resolution in regions between two adjacent jets than the other two meshes. On the other side, Grids 2 and 3 yield practically the same results, indicating that additional mesh refinement near the target plate does not affect the solution. This shows that reducing the near-wall spacing y^+ below one has no impact on the results. Discrepancy between the tested meshes in radial profiles of mean eddy viscosity and mean turbulence kinetic energy is rather small. It may be also observed that very similar mean wall temperature is obtained for all tested meshes. The only notable differences are observed at jets' impingement locations, where a slightly lower wall temperature is obtained for both dense meshes.

The results for both turbulence models, using the Grid 2, are presented in Figure 3. From the mean velocity profiles, it can be observed that SST model predicts slightly slower decay of the central jet than SAS, i.e. the magnitude of the mean axial velocity at jet's axis is higher, with somewhat narrower jet core region. A notable difference may be observed also at $|x/D|{\sim}2$, where somewhat greater bending of both neighbour jets radially outward is observed for the SST model where the inner side of both neighbour jets is suppressed.

Locally, lower levels of eddy viscosity ν_t and modelled turbulence kinetic energy k are obtained with the SAS model. However, the reduction of ν_t in the present case seems to be still insufficient to allow the development of flow unsteadiness. Thus, practically no resolved fluctuations have been detected in the instantaneous flow fields even with the SAS model. It should be noted that approximately one order of magnitude lower $\nu_t$values were detected in LES.

Since both turbulence models predict very similar (instantaneous and mean) flow characteristics near the target wall, practically the same heat transfer characteristics were obtained for both turbulence models. In comparison to LES, approximately 2°K lower mean wall temperature is obtained with the URANS simulations, which can be attributed to the "excessive" levels of modelled eddy viscosity in URANS simulations in comparison to LES.

Based on the Eqs. 3 and 4, the heat transfer rate is proportional to the eddy viscosity which appears in the numerator in the expression for turbulent (eddy) heat diffusivity α_t . Consequently, the increase of ν_t leads to the increase of α_t, and as such also to the effective heat diffusivity α_{eff}. From the mathematical point of view, the effective heat diffusivity can also be modified with a change in the value of turbulent Prandtl number $\mathrm{Pr_t}$ appearing in the denominator of α_t (see Eq. 4). We can use $\mathrm{Pr_t}$ as a parameter to investigate the turbulent heat transfer by directly (and with more control) modifying α_t. Directly modifying $\backslash alpha_t$ via artificially prescribing higher or lower values of $\mathrm{Pr_t}$ helps us to explore the limits of under- and over-predicting heat transfer.

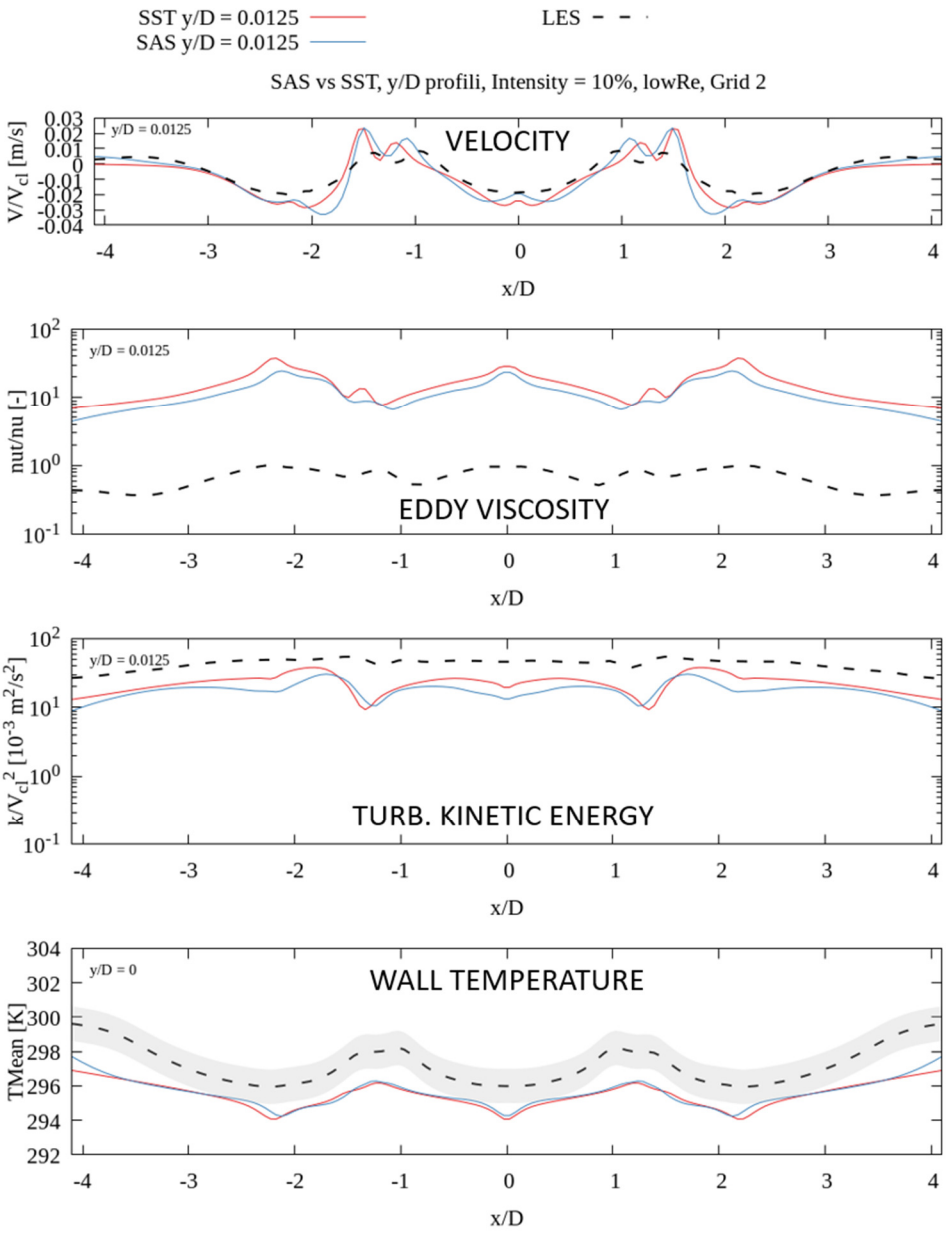

Figure 3: Mean flow characteristics and mean wall temperature.

The following example shows how the heat transfer prediction changes with the variation of turbulent Prandtl number. Since the temperature T is treated as the passive scalar, the momentum and heat transfer equations are decoupled. Thus, any change in thermal properties of air does not affect obtained flow fields, except T.

Figure 4 shows how the predicted mean wall temperature changes with the variation of turbulent Prandtl number, which has been changed from 0.45 to 3.6. The reference value is 0.9. It may be seen that the mean wall temperature changes for approximately 2°K when Pr_t is increased by a factor of 8 (i.e. from 0.45 to 3.6). The change in obtained mean temperature is even higher in the secondary stagnation zones (i.e. at $x/D \sim 1$), where wall-parallel fluid motion is rather weak due to a formation of a fountain flow (thus convective heat transfer is rather low).

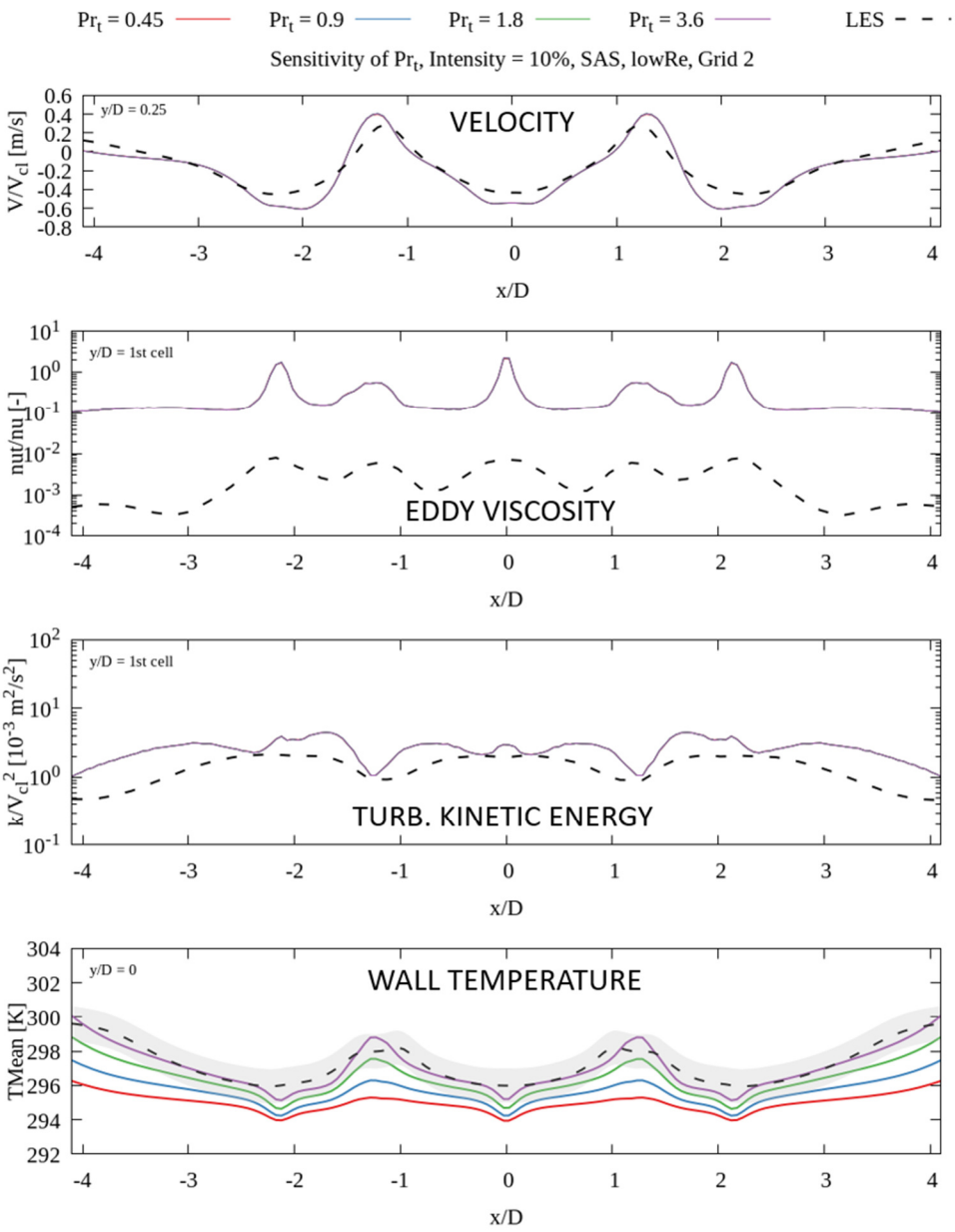

Figure 4: Variation of mean wall temperature due to changes of turbulent Prandtl number.

4 CONCLUSIONS

This work evaluates the capability of two URANS turbulence models for heat transfer predictions of multiple impinging jets at moderate Reynolds numbers. The numerical simulations are conducted with the open-source CFD code OpenFOAM using the SST and SST-SAS turbulence models. Results are validated against the well-resolved LES benchmark [8].

For the present setup, i.e. the discretization schemes used in this study, both turbulence models yield very similar instantaneous flow characteristics. Predicted instantaneous flow fields are rather stable, the flapping of jets is practically negligible, and the flow instabilities that usually develop in the shear layer of turbulent impinging jets are completely suppressed. Since the SST-SAS model predicts very similar mean flow characteristics of turbulent impinging jets as the standard SST model, also the differences in obtained mean heat transfer characteristics between both URANS models are practically negligible. In comparison to LES, higher eddy viscosity values are obtained with both URANS models. Consequently, higher heat

transfer rates are predicted by URANS simulations, resulting in approximately 2°K lower mean temperature of the impingement wall than in LES.

ACKNOWLEDGMENTS

The financial support provided by the Slovenian Research Agency, grants J2-9209, P2-0405 and P2-0026 is gratefully acknowledged.

REFERENCES

[1] M. Draksler, B. Končar, L. Cizelj, B. Ničeno, "Large Eddy Simulation of multiple impinging jets in hexagonal configuration – Flow dynamics and heat transfer characteristics", Int. J. Heat Mass Transfer, 109, pp. 16-27, 2017.

[2] M .Draksler, B. Končar, "On the capability of URANS modelling of multiple impinging jets", Proc. Int. Conf. Nuclear Energy in Central Europe 2017, Bled, Slovenia, September 11-14, Nuclear Society of Slovenia, 2017, pp. 213.1-213.8.

[3] M .Draksler et al., "On The Capability Of Scale-Adaptive Simulation Method for Multiple Impinging Jets", Proc. Int. Conf. Nuclear Energy in Central Europe 2018, Portorož, Slovenia, September 10-13, Nuclear Society of Slovenia, 2018, pp. 317.1-317.7.

[4] M. Draksler et al., On the accuracy of Large Eddy Simulation of multiple impinging jets, Int. J. Heat Mass Transf., 133, pp. 596-605, 2019.

[5] M. Draksler, B. Ničeno, B. Končar, L. Cizelj, "Large eddy simulation of multiple impinging jets in hexagonal configuration - Mean flow characteristics", Int. J. Heat Fluid Flow 46, pp. 147-157, 2014.

[6] https://www.openfoam.com/news/main-news/openfoam-v1812

[7] F.R. Menter, M. Kuntz, and R. Langtry. Ten years of industrial experience with the SST turbulence model. In Proceedings of the fourth international symposium on turbulence, heat and mass transfer, pages 625–632, Antalya, Turkey, 2003. Begell House.

[8] Egorov, Y., & Menter F.R. (2008). Development and Application of SST-SAS Model in the DESIDER Project. Advances in Hybrid RANS-LES Modelling, Notes on Num. Fluid Mech. And Multidisciplinary Design, Volume 97, 261-270.

[9] F. R. Menter, Y. Egorov, "The Scale-Adaptive Simulation Method for Unsteady Turbulent Flow Predictions. Part 1: Theory and Model Description", Flow Turbulence Combust, 85, pp. 113-138, 2010.

[10] Tobias Holzmann. Mathematics, Numerics, Derivations and OpenFOAM(R), Holzmann CFD, Leoben, fourth edition, February 2017. URL www.holzmann-cfd.de.

[11] ANSYS Meshing, ANSYS® Academic Research, Release 2019R1